Electronic Supplementary Information

Fluorescence Microscopy of Single Lead Bromide Nanocrystals Reveals Sharp Transitions during Their Transformation to Methylammonium Lead Bromide

Bo Yin[1], John Cavin[2], Dong Wang[3], Daniel Khan[3], Meikun Shen[3], Craig Laing[3], Rohan Mishra[4,1], Bryce Sadtler[3,1]*

[1]Institute of Materials Science & Engineering, Washington University, St. Louis, Missouri 63130

[2]Department of Physics, Washington University, St. Louis, Missouri 63130

[3]Department of Chemistry, Washington University, St. Louis, Missouri 63130

[4]Department of Mechanical Engineering and Materials Science, Washington University, St. Louis, Missouri 63130

* To whom correspondence should be addressed. Email: sadtler@wustl.edu

Materials and Methods

Materials: Lead(II) oxide (PbO, ≥ 99.9%), tetrabutylammonium bromide (TBAB, ≥ 98%), oleylamine (OLA, 70%), methylamine solution (CH_3NH_2, 33 wt. % in absolute ethanol), oleic acid (90%), 2-propanol (IPA, anhydrous, 99.5%), tert-butanol (anhydrous, ≥ 99.5%) and toluene (anhydrous, 99.8%) were purchased from Sigma-Aldrich Inc. 1-octadecene (ODE, tech. 90%) and hydrobromic acid (HBr, ACS 47.0 – 49 %) were purchased from Alfa Aesar. All chemicals were used as received.

Synthesis of lead bromide ($PbBr_2$) nanocrystals: The procedure for synthesizing $PbBr_2$ nanocrystals was adapted from a previous report.[1] In a typical reaction, a two-flask method was used in which Flask (I) contained the bromide precursor and Flask (II) contained the lead precursor. A Schlenk line system was used in the synthesis to evacuate each flask and put it under an environment of N_2. In Flask (I), 2 mmol of TBAB was used as the bromide precursor and mixed with OLA (5 mL) and ODE (5 mL). Note that TBAB does not dissolve in this solvent system until after heating. Flask (I) was evacuated using a Schlenk line to a pressure below 150 milliTorr, heated to 120°C, and held at this temperature while stirring for 90 min to remove water and oxygen. Subsequently, Flask (I) was switched from vacuum to a N_2 environment and heated to 200°C for 60 min. At this point the solution in Flask (I) turned clear indicating that the TBAB had dissolved. The heating source was then removed to allow Flask (I) to cool. Once the temperature of Flask (I) reached 50°C, it was kept at this temperature to avoid solidification. In Flask (II), 1 mmol of PbO used as the lead precursor, 1 mL (3 mmol) of oleic acid, and 15 mL of ODE were mixed together with stirring. Similar to Flask (I), Flask (II) was put under vacuum and heated to 100°C for 90 min with stirring to remove water and oxygen. Then Flask (II) was allowed to cool to 80°C under a N_2 environment, where it was kept at this temperature for 60 min. At this point, the mixture in Flask (II) turned clear and colorless. While still under a N_2 environment, the temperature of Flask (II) was then raised to 200°C. After the temperature of Flask (II) stabilized at 200°C, the solution from Flask (I) was injected into Flask (II) with vigorous stirring. After mixing the contents of the two flasks, the reaction was kept at 200°C for 15 min and then removed the heating source. The solution in Flask (II) was clear and colorless at this point. Next, 10 mL of anhydrous toluene was injected into Flask (II) to cool the reaction solution. After Flask (II) cooled to room temperature, the product solution was stored in an argon-filled glovebox for future use. Over a 24-hour period,

a white precipitate formed in Flask (II). This precipitate was determined to be Pb(OH)Br by x-ray diffraction, while the clear supernatant contained only $PbBr_2$ nanocrystals as determined by x-ray diffraction, electron diffraction, and x-ray photoelectron spectroscopy.

Washing procedure for $PbBr_2$ nanocrystals: We found that solutions of $PbBr_2$ nanocrystals remained stable for longer periods of time (up to 6 months) by keeping the nanocrystals in the original reaction solution. Therefore, individual aliquots were washed prior to characterization. In a typical washing procedure, 1 mL of anhydrous 2-propanol was added to 0.2 mL of the clear supernatant of the $PbBr_2$ reaction solution in a glovebox. After thoroughly mixing the solution, the nanocrystals began to precipitate as a white powder. The solution was transferred to a centrifuge tube, taken out of the glovebox, and centrifuged at 5,000 rpm for 5 min. The centrifuge tube was then brought back into the glovebox, and the supernatant was removed. Next, 6 mL of anhydrous toluene were added to the white precipitate. After mixing, the white precipitate dispersed back to form a clear colloidal solution. This solution could be used to characterize the nanocrystals by TEM, UV-Visible absorption, and photoluminescence spectroscopy. For characterization by x-ray diffraction and x-ray photoelectron spectroscopy, the sample was washed twice using the procedure described above and dispersed in isopropanol rather than toluene.

Synthesis of methylammonium bromide (CH_3NH_3Br): Methylammonium bromide (CH_3NH_3Br) was synthesized following a previously reported procedure for making CH_3NH_3I (except HBr was used instead of HI).[2] First, 24 mL of a CH_3NH_2 solution (33 wt. % in ethanol) was reacted with 10 mL of HBr (47-49%) in 100 mL ethanol. After the reaction, a rotary evaporator was used to remove ethanol and isolate the resulting CH_3NH_3Br powder. The white CH_3NH_3Br powder was

collected and further dried in a vacuum oven at 60°C overnight. The CH_3NH_3Br powder was stored in a glovebox for future use.

Characterization:

To prepare samples for x-ray diffraction (XRD), several drops of the washed nanocrystals (dispersed in anhydrous 2-propanol) were drop-cast onto a zero-background, silicon diffraction plate (MTI Corporation). The solution was allowed to dry on the diffraction plate in a glovebox. XRD patterns were then collected using a Bruker D8 Advance X- ray Diffractometer (Cu Kα = 0.154 nm). The step size for the XRD measurements was 0.02° in 2θ, and the scan rate was 0.5 s per step.

X-ray photoelectron spectroscopy (XPS) was performed using a Physical Electronics 5000 VersaProbe II Scanning ESCA (XPS) Microprobe system with a base pressure below 1×10^{-9} Torr. XPS data were acquired using the 1486.6 eV line from a monochromated Al Kα source at 150 W with a multichannel detector set to a pass energy of 23.5 eV for the high-resolution scans. The expected peak positions and chemical shifts were obtained from the National Institute of Standards and Technology (NIST) X-ray Photoelectron Spectroscopy Database.[3]

To obtain ensemble optical spectra of the $PbBr_2$ nanocrystals after different amounts of CH_3NH_3Br were added to the solution (see **Figure 2** in the main manuscript), the nanocrystals were prepared in the following manner. An aliquot of the $PbBr_2$ nanocrystals after washing as described above was further diluted by a factor of approximately 2.5. For example, 10 mL of the washed solution was diluted to 25 mL solution with anhydrous toluene. For each titration, 3 mL of the diluted solution was added to a quartz cuvette. Next, the following amounts of a CH_3NH_3Br solution (0.55 mg/mL in anhydrous IPA) were added to each cuvette: 10 μL, 20 μL, 30 μL, 60 μL,

90 μL, and 180 μL. The UV-Vis absorption and photoluminescence spectra were measured immediately after addition of the CH_3NH_3Br solution. When 180 μL of the solution was added, no obvious changes in the absorption edge of the nanocrystals were observed compared to when 90 μL was added. Thus, we considered the nanocrystals to be completely transformed to $CH_3NH_3PbBr_3$ using the 90 μL aliquot.

UV−Vis absorption spectra were measured using a Perkin-Elmer Lambda 950 spectrometer equipped with a 150-mm, integrating sphere, a PMT detector, a tungsten halogen lamp for the visible region (350–800 nm), and a deuterium lamp for the ultraviolet region (250–350 nm). Each cuvette was placed at the front entrance of the integrating sphere to measure the transmitted light. The scan rate for each measurement was 266.75 nm/min, and the step size was 1.0 nm.

Photoluminescence spectra were recorded using a Cary Eclipse fluorescence spectrophotometer. Photoluminescence spectra were collected from 450 nm to 600 nm. The scan rate for each spectrum was 600 nm/min, and the step size was 1 nm. The excitation wavelength was 400 nm for all samples except for the 90 μL aliquot. For this sample, an excitation wavelength of 400 nm gave an emission intensity that was greater than the detection limit. The excitation wavelength was increased to 475 nm to reduce the emission intensity of the 90 μL aliquot.

Transmission electron microscopy (TEM) was performed using a JEOL 2000FX transmission electron microscope with an acceleration voltage of 200 kV using a LaB6 filament as the electron source. After washing, a drop of the nanocrystal solution was drop-cast onto a TEM grid (Ted Pella, Inc #01811). Electron diffraction patterns were obtained using a more concentrated solution of nanocrystals. The camera length was 150 cm.

Flow cell preparation: Home-made flow cells were used for all fluorescence microscopy experiments. The preparation followed a procedure described by Chen and coworkers with some modifications.[22] The flow cells consisted of a top glass slide (25 × 75 mm, 1.0 mm thick) and a bottom coverslip (24 × 50 mm, #1.5). For the top glass slide, two holes (1 mm in diameter with a 25-mm separation) were drilled to allow for liquid to flow in and out of the flow cell. The holes were drilled by immersing the slide in water and using a 1 mm, diamond-coated drill bit at speed of approximately 25 kRPM using a dremel (DREMEL 4000). Before use, the drilled glass slides were cleaned by sonicating in acetone for 30 min and dried using N_2 gas.

The $PbBr_2$ nanocrystals were first spin-coated onto the bottom coverslip before assembling the flow cell. In order to achieve a uniform dispersion of single nanocrystals on the coverslips, we found that the solution of $PbBr_2$ nanocrystals needed to be diluted by a factor of approximately 3200 compared to the as-synthesized sample in solution. Anhydrous toluene was originally used to dilute the $PbBr_2$ solution. However, toluene has a relatively large contact angle on the glass coverslips, which often led to a non-uniform dispersion of nanocrystals. To improve the dispersion, a mixture of anhydrous toluene and anhydrous IPA was used to lower the contact angle. When the volume ratio between toluene and IPA was 3:1, a uniform dispersion of $PbBr_2$ nanocrystals on the coverslips was achieved.

To assemble a flow cell, two polytetrafluoroethylene (PTFE) tubes (Cole-Parmer, 1/32" ID × 1/16" OD) were first attached to the holes of the top glass slide. Epoxy (Gorilla 5 min epoxy) was used to seal around the tubes, and the epoxy was allowed to cure for at least 180 min. After curing, double-sided tape (3M) was placed on the top glass slide to form a rectangular shaped flow channel surrounding the two drilled holes. The bottom coverslip was then adhered to the tape with the nanocrystals facing in between the two slides. The height of the flow channel was defined by the

thickness of the double-sided tape, which was about 60 μm. The volume of the channel was approximately 6 μL. Then epoxy was applied around the double-sided tape to create a liquid-tight seal. The epoxy was allowed to dry and solidify under vacuum for at least 60 min before conducting the microscopy experiments described below.

Single-nanocrystal reaction trajectories: Single-nanocrystal fluorescence imaging was carried out using a Nikon N-STORM microscopy system consisting of a Nikon TiE motorized inverted optical microscope and a Nikon CFI-6-APO TIRF 100× oil-immersion objective lens with a numerical aperture of 1.49 and a working distance of 210 μm. The microscope also contains optics for imaging using differential interference contrast (DIC), which was used for rough focusing of the top of the coverslip. The microscope was then switched to fluorescence mode with a long exposure time (1 s) to bring the coverslip into fine focus. The Nikon Perfect Focus 3 system was used to maintain focal stability during imaging. As shown in **Scheme 1** of the main manuscript, the nanocrystals on the bottom coverslip of the flow cell were photoexcited by sending filtered light from a white light-emitting diode (LED) through the objective. The irradiance near the focal plane was measured to be 155 μW/cm^2. A filter cube was used (Chroma, set #49002) with an excitation filter that had 90% transmission for blue light of wavelengths between 450 and 480 nm. The emission filter had 90% transmission between 500 and 540 nm, while the photoluminescence maximum for a solution of the $CH_3NH_3PbBr_3$ nanocrystals was ~510 nm. A dichroic mirror in the filter cube with a cutoff wavelength of 500 nm was used to separate the excitation and emission. An Andor iXon 897 electron-multiplying CCD with single photon sensitivity (512 × 512, 16 μm pixels, 90% quantum efficiency) was used to detect the fluorescent signals. The time resolution

of the EMCCD camera is 0.02 s, which means the camera will take 50 measurements in 1 s. Images were collected with an exposure time of 2 ms.

During a typical experiment, the entrance tube of the flow cell was connected to one end of a three-way tee connection (Cole-Parmer, tube OD 1 to 4 mm). The other two ends of the three-way tee were each connected to a syringe pump. One syringe pump was used to inject 1-octadecene (ODE) while the other syringe pump was used to introduce the CH_3NH_3Br solution. CH_3NH_3Br at different concentrations was dissolved in a mixture of tert-butanol and ODE with a volume ratio of 2:3. Before imaging the transformation of the nanocrystals, pure ODE was injected into the flow cell at a typical injection rate of 7.5 mL/h. The focus of the microscope was then readjusted to the top surface of the coverslip where the nanocrystals were located. After focusing, the addition of pure ODE was stopped, and the CH_3NH_3Br reactant solution was injected at a rate of 5 mL/h. Switching between the two syringe pumps would create a small air bubble in the PTFE tube, which was used as a marker for the flow of the CH_3NH_3Br solution. The air bubble also prevented dilution of the CH_3NH_3Br solution into the pure ODE solution. Recording of the fluorescence video began when the air bubble was close to entering the flow cell.

Data Analysis: All fluorescence microscopy videos (time-stacks of images) were recorded using Nikon Elements software (Advanced Research 4.50). Nikon Elements is equipped with basic analysis functions. For example, the intensity trajectory for the entire field-of-view (wide-field intensity in **Figure 3e**) could be directly measured using this software. Single nanocrystals were identified manually from the stack of image frames. Regions of interest (ROIs) were defined around single emitting nanocrystals where no intensity from nearby nanocrystals was present. Intensity trajectories from these ROIs were then measured using the Nikon Elements software, and

the data was exported into an Excel spreadsheet. The following data processing was then performed using MATLAB.

Waiting time analysis: For each single-nanocrystal trajectory, the waiting time was measured as the time needed for the fluorescence intensity to reach a threshold value. The threshold intensity value, V, is given by the following equation:

$$V = m + 6 \times \sigma \quad (1)$$

where m is the mean value of the intensity before the reaction started, and σ is the standard deviation of a Gaussian fit to the noise. For a given ROI, the m and σ values were determined using 2 s of the video (100 recorded points in the video) at a time point before the nanocrystal started to "turn on" (i.e., before the fluorescence intensity began to increase). Gaussian fitting of the distributions of waiting times were performed in Origin. For each experiment, the video recording started when the air bubble formed after switching solutions entered the flow cell. As the region observed in the flow cell varied for each recording, the time at which the first nanocrystal was observed to turn on after the recording started could vary by a few seconds even when the same concentration of CH_3NH_3Br was used. When multiple videos were recorded at a single concentration, the Gaussian fits were aligned based on the mean value of the fits. After aligning the histograms, the first nanocrystal to transform was given a relative waiting time of 0 s. Thus, the waiting times were measured relative to the time when the first nanocrystal was observed to transform.

The same criterion was applied to determine the start-time for the ensemble of $PbBr_2$ nanocrystals to transform. First, 100 recorded intensity points (i.e., 2 s of recording) were used to calculate the m and σ values over the entire field-of-view. The start-time was calculated as the

time point at which the intensity reached the value V given in equation 1. Once the intensity had stabilized after introducing the CH_3NH_3Br solution, the mean intensity over the entire field-of-view was again calculated using 100 recorded points. The end-time for completion of the ensemble transformation was calculated as the time point at which the intensity reached 90% of this final mean value. The ensemble reaction time was then taken as the difference between the start-time and end-time. The ensemble reaction times for different concentrations of CH_3NH_3Br are shown in **Table S1** below.

Switching time, τ, analysis: For each individual nanocrystal, the switching time, τ, was determined by fitting a segment of its intensity trajectory, $I(t)$, to a sigmoidal function:

$$I(t) = I_{initial} + \frac{\left(I_{final} - I_{initial}\right)}{1 + exp\{(b - t)/\tau\}} \tag{2}$$

where $I_{initial}$ is the mean intensity value of the baseline at the start of the trajectory (i.e. the value of m in equation 1), I_{final} is the mean intensity value at the end of the fitted segment when the intensity value was stable, and b and τ are parameters that were fit using MATLAB.

Monte Carlo Simulations: The general set up of all our models was the same. We used an ensemble of 400 nanocrystals each consisting of 20 sites where ion intercalation can occur. In our models, we did not distinguish between methylammonium and bromide ions. At each time step a nanocrystal is chosen at random. Intercalation of an i^{th} ion occurs with a probability p_i that is varied to simulate different transformation models. If 20 ions have already been intercalated into a nanocrystal, then intercalation automatically fails. After an intercalation succeeds or fails, the simulation time is increased by one, and the process repeats until the ensemble average of

intercalated ions reaches a certain threshold. The simulation ended when the average number of intercalation events for each particle among the ensemble was 19.98.

The details of the model lie in the probability of ion intercalation p_i. Here p_i is determined through the equilibrium constant k_i of each reaction, which is in turn determined by the net free energy change, ΔG_i, associated with an intercalation event. The relationship between the equilibrium constant and the free energy change for the i^{th} intercalation is given by the following:

$$k_i = exp\left(-\frac{\Delta G_i}{kT}\right) \tag{3}$$

where k is the Boltzmann constant and T is the temperature. For positive ΔG_i, the probability of intercalation is then given by the following:

$$p_i = \frac{k_i}{1 + k_i} \tag{4}$$

When ΔG_i is negative however, the reaction becomes favorable and is no longer determined by an equilibrium process, such that $p_i = 1$.

Each model then is reduced to a function of ΔG_i, which can be varied to simulate various pathways for the nanocrystal transformation. We have used five different physical models that describe how intercalation events are affected by ions that have already been intercalated. For all our models, we assume that the energetic cost for the first intercalation is the same: ΔG_1 with an associated $k_1 = 0.03$. ΔG_i can therefore be thought of as a constant energetic cost plus an ion-dependent term, Δg_i, associated with the specific model in question:

$$\Delta G_i = \Delta G_1 + \Delta g_i \tag{5}$$

In order to simulate the effects of intercalation events being less likely after many intercalations in a nanocrystal due to a lack of empty sites, we include a probability of failure proportional to the number of intercalated ions. The adjusted p_i has the following form:

$$p_i = \frac{k_i}{1 + k_i}\left(1 - \frac{i - 1}{20}\right) \tag{6}$$

Below we outline five proposed models of the mechanics of ion intercalation in $PbBr_2$ nanocrystals. Each model consists of a physical interpretation and a mathematical description of Δg_i. The value of ΔG_i is the same for each model. **Figure S9** shows the free energy change associated with each of the 20 intercalation events and their corresponding probabilities for these models.

Diffusion Limited: This model can be considered to be the control case. In it, ion intercalation is purely diffusion limited such that previous intercalations bear no consequence for future intercalations. In this case the energy required to intercalate is constant, and so $\Delta g_i = 0$.

Positive Cooperativity: Routzahn and Jain previously studied cation exchange in CdSe nanocrystals using single-nanocrystal fluorescence.[4] As in our system, individual fluorescence trajectories in CdSe nanocrystals exhibited much shorter switching times than the ensemble. They proposed positive cooperativity as an explanation for this phenomenon. In positive cooperativity, each additional ion exchanged/intercalated reduces the energy of the next event by a constant amount. The result is a Δg_i term that decreases linearly with i:

$$\Delta g_i = -\alpha i \tag{7}$$

In this expression, α is a proportionality factor that corresponds to the free energy reduction for intercalation events for every previous swap. Using this model in their simulations, they were able to reproduce abrupt nanocrystal transformations with a distribution of waiting times corresponding to slower kinetics for the ensemble.

Continuous Nucleation: This model is an adaptation of the classical nucleation model where the growth of a new phase is determined by a radius (r)-dependent change in free energy, $\Delta G_{classical}(r)$:

$$\Delta G_{classical}(r) = \alpha_{classical} r^2 - \beta_{classical} r^3 \quad (8)$$

Growth is encouraged by a term proportional to volume with $\beta_{classical}$ being the binding energy-related proportionality constant and discouraged by a term proportional to surface area with $\alpha_{\text{classical}}$ being the surface tension-related proportionality constant. Thus, there is a critical radius, r_c, at the maximum in free energy after which growth is energetically favorable:

$$r_c = \frac{2\alpha_{classical}}{3\beta_{classical}} \quad (9)$$

In order to begin mapping this problem onto the nanocrystal transformation we replace the radius dependence with a volume (V) one by assuming a spherical shape:

$$\Delta G_{classical}(V) = \alpha_{classical} \left(\frac{3}{4\pi} V\right)^{2/3} - \beta_{classical} \left(\frac{3}{4\pi} V\right) \quad (10)$$

Since the volume of the new $CH_3NH_3PbBr_3$ phase is proportional to the number of previous intercalation events, we replace V with i and the classical coefficients and prefactors of equation 10 with nanocrystal ones giving:

$$\Delta G_{NC}(i) = \alpha'_{NC}(i)^{2/3} - \beta_{NC} i \quad (11)$$

However, this gives the total change in free energy from the pristine nanocrystal, and we want the change at each intercalation event. Differentiating equation 11 with respect to i, we obtain:

$$\Delta G_i = \alpha_{NC}(i)^{(-1/3)} - \beta_{NC} \quad (12)$$

Setting $i = 1$, we obtain $\Delta G_1 = \alpha_{NC} - \beta_{NC}$. From this, equation 5, and equation 12, we arrive at an expression for the ion-dependent term in the change in free energy:

$$\Delta g_i = \alpha_{NC}\left(i^{(-1/3)} - 1\right) \tag{13}$$

Qualitatively, Δg_i starts at 0 and it approaches $-\alpha_{NC}$. The intercalation event, i_c, that corresponds to $\Delta g_{i_c} = -\Delta G_1$ is analogous to the critical radius, r_c. At this point, intercalation is favorable and governed by a non-equilibrium process.

Sudden Nucleation: This model is similar to the continuous nucleation case except that $\Delta g_i = 0$ (i.e., diffusion-limited growth), until a transition point is reached when Δg_i suddenly drops to $-\alpha$ with $\alpha > \Delta G_1$. Typical applications of the classical nucleation model involve using thermodynamics and the height of the energetic barrier in equation 10 to predict the statistics of the time for the nucleating phase to reach the critical size. In the previous continuous nucleation model for nanocrystals, this is replaced by step-by-step growth determined by the free energy curve of the barrier. In the sudden nucleation model, the connection to classical nucleation comes from a statistical time-scale for non-equilibrium growth to start determined by an energetic barrier: ΔG_1 in this case. In our simulations using this model, we defined the critical point to be at 25% maximum ion intercalation, 5 in this case. After this point, intercalation events become much more probable.

Phase Transformation and Nucleation: The structures of $PbBr_2$ and $CH_3NH_3PbBr_3$ are not related by symmetry operations, that is they lack group–subgroup relations. Therefore, the transformation must proceed through reconstructive transitions. In this model, intercalation is assumed to be diffusion limited until a critical point after which a perovskite phase is adopted. At this point, the presence of many $CH_3NH_3^+$ and Br^- vacancy sites in the perovskite structure is expected to favor additional ion intercalation. Hence, we have used a continuous nucleation model to simulate the

further growth of $CH_3NH_3PbBr_3$ within this perovskite structure. In our simulations, we set the critical point at 20% maximum ion intercalation, 4 in this case.

Supplementary Discussion

XPS analysis: **Figure S3a**, **b** below shows x-ray photoelectron spectra in the binding energy regions for Pb 4f and Br 3d electrons, respectively. After baseline subtraction, the binding energy of the Pb $4f_{7/2}$ peak (lower binding energy peak in **Figure S3a**) is 139.0 eV, and the binding energy of the Br 3d peak is 68.8 eV. The binding energy ranges provided in the National Institute of Standards and Technology (NIST) X-ray Photoelectron Spectroscopy Database are 138.5eV to 139.0 eV for Pb^{2+} in a lead halide and 68.5 eV to 69.0 eV for Br^- in $PbBr_2$.[3] Therefore, the spectra obtained for the nanocrystals match the expected photoelectron spectra for $PbBr_2$.

Effects of flow rate and diffusion: The waiting time is an important parameter extracted from single-nanocrystal intensity trajectories. **Figure 4** of the main manuscript shows that the distribution of waiting times narrows as the concentration of CH_3NH_3Br used to transform the $PbBr_2$ nanocrystals increases. To apply the phase-transformation model to this reaction as discussed in the main manuscript, other factors that could affect the distribution of waiting times need to be excluded, such as gradients in the concentration of CH_3NH_3Br. Under ideal conditions, the same concentration of CH_3NH_3Br should contact all $PbBr_2$ nanocrystals within the field-of-view simultaneously. If the flow rate of the CH_3NH_3Br solution in the micro-flow cell is much faster than the diffusion rate of CH_3NH_3Br, then the effect of CH_3NH_3Br diffusion will be minimized. Based on the cross-sectional area of the flow cell (60 μm by 4 mm), a flow rate of 5 mL/h (the typical flow rate used in these experiments) gives a linear flow velocity of 0.58 cm/s.

While we do not know the diffusion coefficients for $CH_3NH_3^+$ and Br^- in the mixture of ODE and t-butanol, the diffusion coefficients of these ions in water at infinite dilution are 1.56×10^{-5} cm^2/s for $CH_3NH_3^+$ and 2.08×10^{-5} cm^2/s for Br^-.[5] These diffusion coefficients give a root mean square displacement of approximately 0.006 cm in one second, suggesting that the forced flow of the CH_3NH_3Br solution dominates over diffusion.

To verify that a concentration gradient of CH_3NH_3Br is not responsible for the distribution of waiting times at a flow rate of 5 mL/h, **Figure S5** below shows the relation between the position of different individual nanocrystals within the same field-of-view and their measured waiting time. The locations of the nanocrystals are represented by the pixel positions of the CCD camera along the x- (**Figure S5a**) and y-direction (**Figure S5b**), respectively. As shown in these plots, there is no obvious correlation between the waiting times of individual nanocrystals and their locations.

If the incorporation of $CH_3NH_3^+$ and Br^- ions into the nanocrystal lattice is much faster than the diffusion rate of these ions in solution, then their concentration will become depleted near the surface of the nanocrystal. The interdiffusion coefficient of Br^- and Cl^- anions in the related lead halide perovskite compound, $CsPbCl_{3-x}Br_x$, was recently measured to be 2.1×10^{-13} cm^2/s at 298 K,[6] which is 8 orders of magnitude smaller than the diffusion coefficients of these halide ions in aqueous solution.[5] While we do not know the exact diffusion coefficients of $CH_3NH_3^+$ and Br^- ions in either the ODE/t-butanol solvent system or within the transforming $PbBr_2$ lattice, these values suggest a large difference between diffusion in solution and in the solid-state. Therefore, in our simulations we did not include the effect of reactant depletion at the nanocrystal surface.

Effects of light intensity: **Figure S8** below shows a histogram of the relative waiting times for the transformation of $PbBr_2$ nanocrystals using excitation with blue light at an approximate intensity

of 200 μW/cm^2. The CH_3NH_3Br concentration was 0.4 mg/mL. The histograms shown in **Figure 4** of the main manuscript used a light intensity of 155 μW/cm^2. Comparing **Figure S8** and **Figure 4b**, which used the same CH_3NH_3Br concentration, the distributions of the waiting times do not appear to be affected significantly by the light intensity. The median waiting time for the histogram shown in **Figure S8** is 1.94 s, and the median waiting time at the lower light intensity is 1.86 s (see **Figure 5b**). Also, the average switching time using 0.4 mg/mL of CH_3NH_3Br at an intensity of 200 μW/cm^2 is 0.94 ± 0.16 s (average ± 1st standard deviation), while it is 0.90 ± 0.13 s for the same CH_3NH_3Br concentration at an intensity of 155 μW/cm^2 (see **Figure 5b**). Therefore, the two kinetic parameters extracted from the single-nanocrystal intensity trajectories do not depend on light intensity for the intensities used in these experiments.

Simulated waiting and switching times: **Figure S11** shows the median waiting times and switching times for the diffusion-limited, positive-cooperativity, and phase-transformation models of ion intercalation. In a simulation, the waiting time was defined as the time required to reach 50% ion intercalation. This is a stricter definition than we used for the experimental data and ensures that the waiting time accurately reflects the time interval before growth accelerates. In contrast, the switching time was defined similarly in the model as in the experiment as half of the time step difference between 75% and 25% ion intercalation. The data in **Figure S11** reflect the median switching and waiting times for an ensemble of 600 nanocrystals with error bars corresponding to the standard deviations.

An inverse proportionality fit with an added constant, h_i, was applied to both sets of data in each panel of **Figure S11**. The added constant is a result of there being a hard limit in the simulation for how quickly a nanocrystal can be intercalated with ions and an expected limit based

on the size of the ensemble and the intercalation probabilities. The inverse proportionality is from the fact that the time between subsequent intercalation events at a nanocrystal is inversely proportional to the probability of intercalation and that intercalation probability is proportional to concentration k_0 in the limit of small k_0.

$$k_i = k_0 h_i \tag{14}$$

$$p_i = \frac{k_0 h_i}{1 + k_0 h_i} \approx k_0 h_i \tag{15}$$

Figure S11a shows how in the diffusion-limited model, the median waiting and switching times scale at the same rate with respect to concentration. Whereas in **Figure S11b,c** it is shown that the switching times scale much slower than the waiting times in the positive-cooperativity and phase-transformation models, respectively. In fact, the phase-transformation model predicts that the median switching time is nearly constant with respect to concentration in agreement with the experimental results shown in **Figure 5b** of the main manuscript indicating the model's validity.

Supplementary Figures and Table

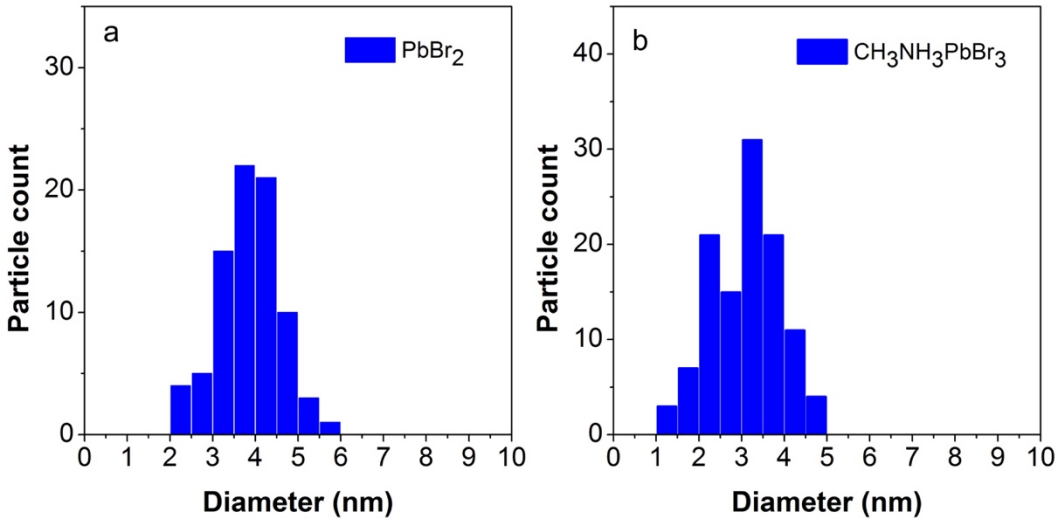

Figure S1. Histograms showing the size distribution of (a) $PbBr_2$ and (b) $CH_3NH_3PbBr_3$ nanocrystals measured using TEM images for the same samples shown in **Figure 1** of the main manuscript.

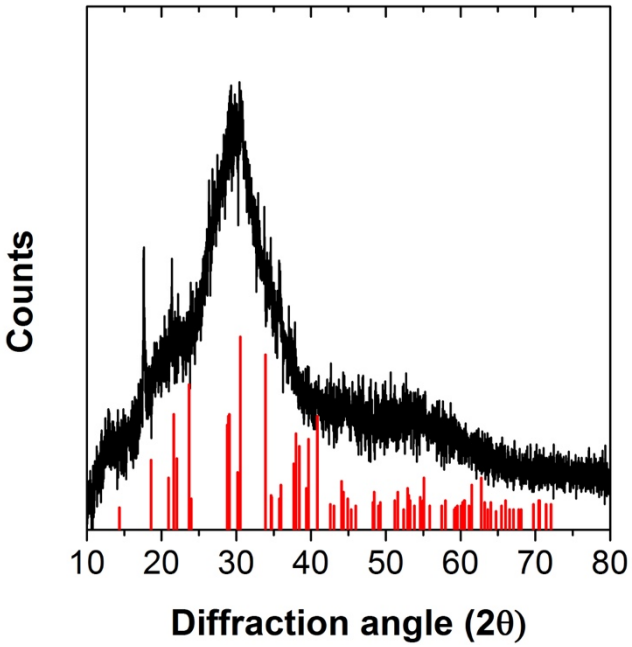

Figure S2. XRD pattern of the as-synthesized nanocrystals dried on a zero-background, silicon diffraction plate. The pattern obtained from a bare Si diffraction plate was subtracted from the sample pattern. The red lines correspond to the reflections for a standard XRD powder pattern of $PbBr_2$ (PDF card # 031-0679).

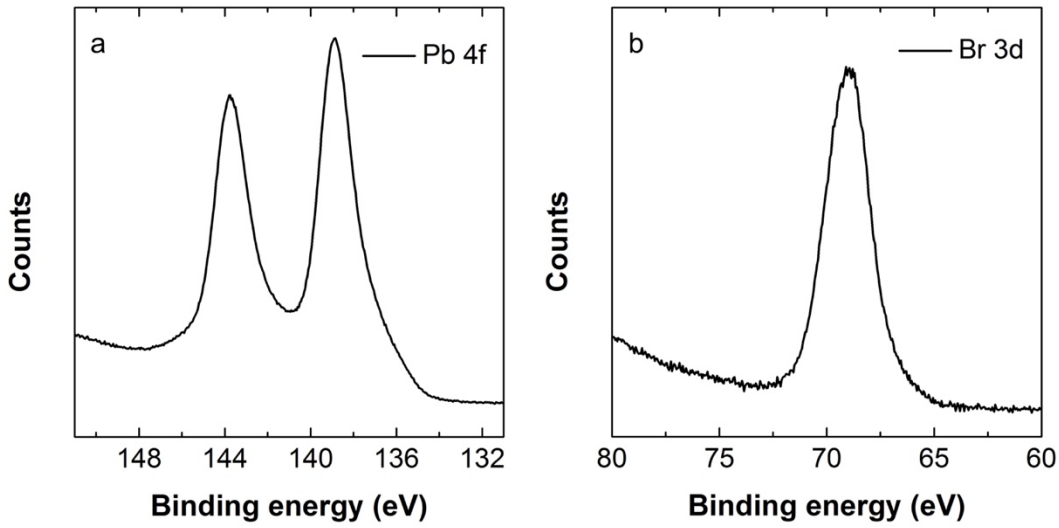

Figure S3. X-ray photoelectron spectra of the as-synthesized $PbBr_2$ nanocrystals showing the binding energy regions for (a) Pb 4f electrons and (b) Br 3d electrons.

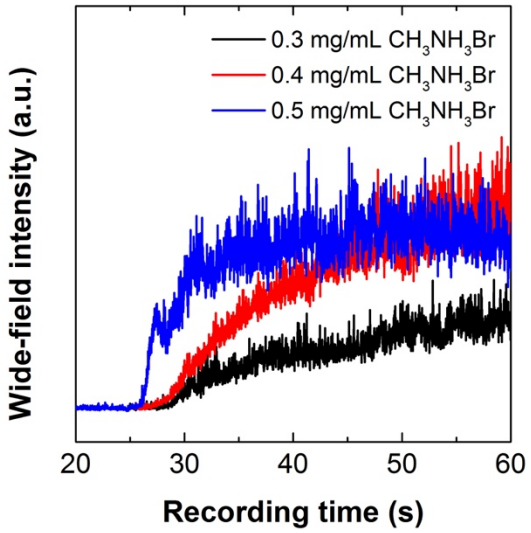

Figure S4. The integrated fluorescence intensity versus time over the entire field-of-view recorded after injecting CH_3NH_3Br into flow cells containing $PbBr_2$ nanocrystals. The concentration dependence of the transformation averaged over the entire the field-of-view is seen by a sharper rise in fluorescence intensity for higher concentrations of CH_3NH_3Br.

Table S1. Comparison of the intensity rise over the entire field-of-view to the average single-nanocrystal switching time using different concentrations of CH_3NH_3Br.

CH_3NH_3Br concentration	0.3 mg/mL	0.4 mg/mL	0.5 mg/mL	1.0 mg/mL
Ensemble reaction time	24.8 s	17.3 s	4.7 s	6.9 s
Average single-nanocrystal switching time	0.88 s	0.82 s	0.90 s	1.00 s

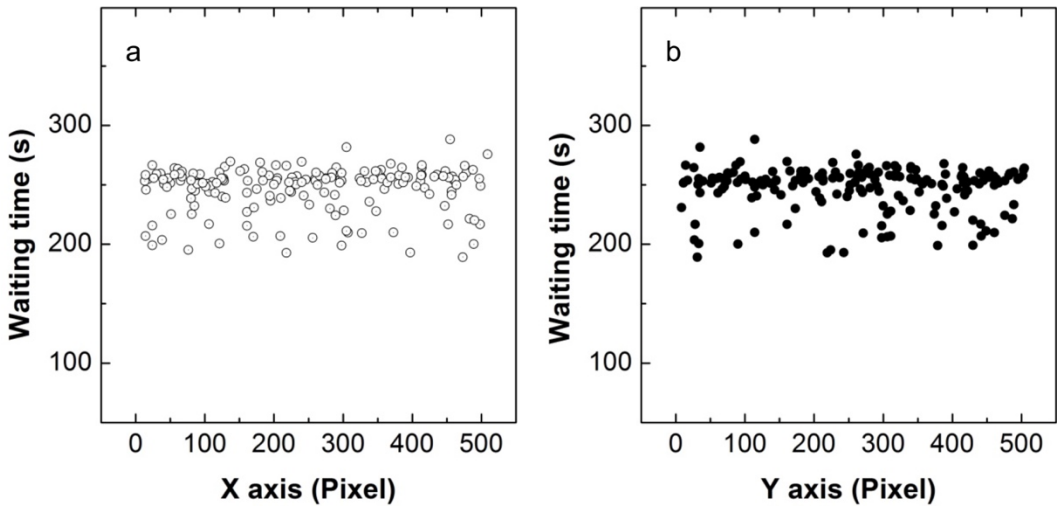

Figure S5. The waiting times for different nanocrystals within the same field-of-view plotted vs. their location. The abscissa in (a) and (b) correspond to the pixel position of the CCD camera along the x- and y-direction, respectively.

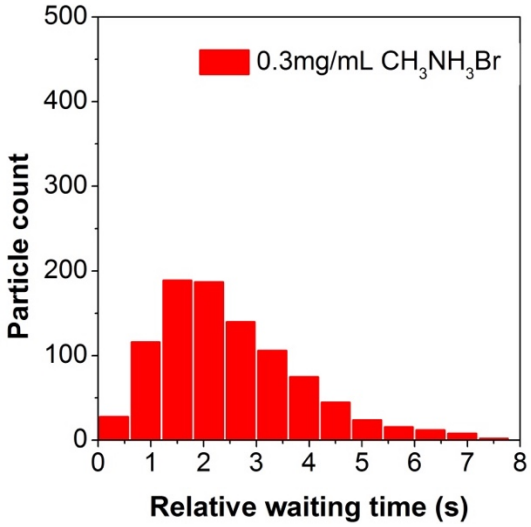

Figure S6. Histogram of the relative waiting times for $PbBr_2$ nanocrystals to transform into $CH_3NH_3PbBr_3$ when the concentration of CH_3NH_3Br was 0.3 mg/mL. The first nanocrystal observed to transform was set to a relative waiting time of 0 s in this plot.

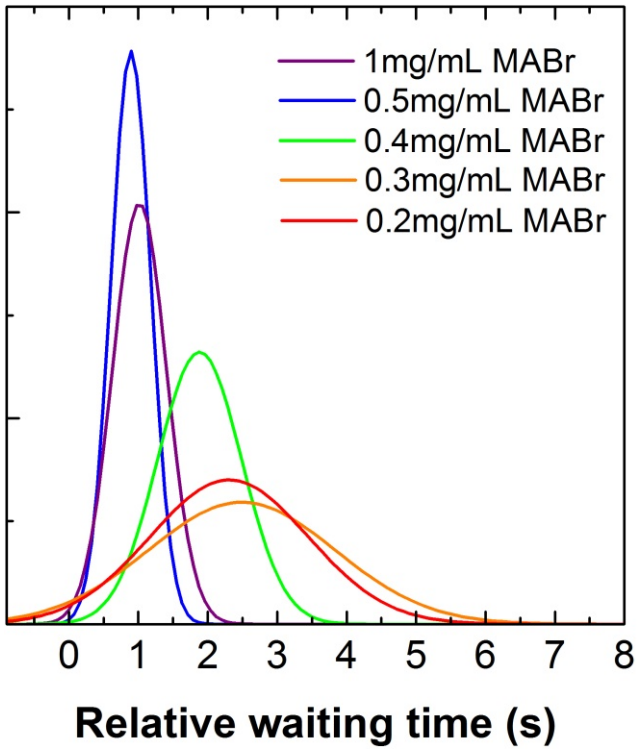

Figure S7. Fittings of the distributions of waiting times shown in **Figure 4** and **Figure S6** at different concentrations of CH_3NH_3Br (MABr) to Gaussian distributions.

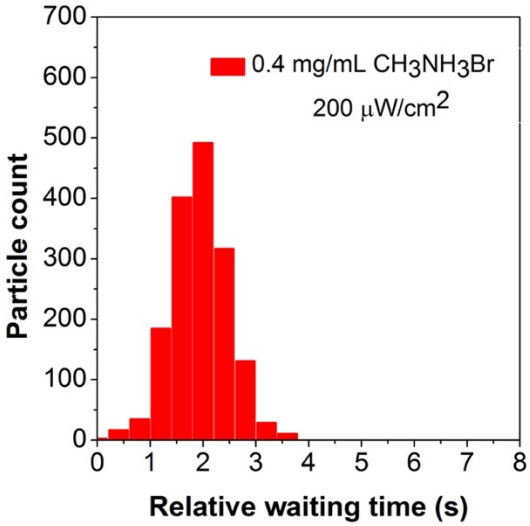

Figure S8. Histogram of the relative waiting times for $PbBr_2$ nanocrystals to transform into $CH_3NH_3PbBr_3$ conducted at a higher light intensity than the histograms shown in **Figure 4**. The concentration of CH_3NH_3Br was 0.4 mg/mL, and the irradiance near the focal plane was 200 $\mu W/cm^2$. The first nanocrystal observed to transform was set to a relative waiting time of 0 s in this plot.

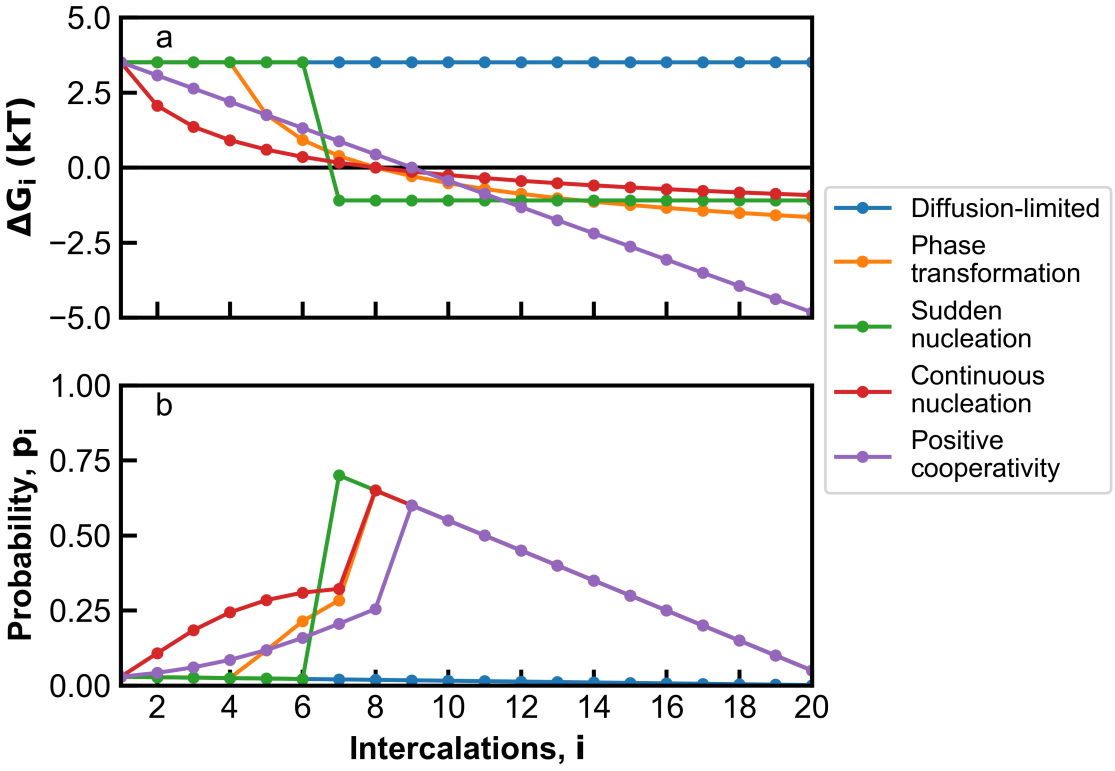

Figure S9. Free energy change and probability associated with successful intercalation for all five models. Panel (a) shows the change of free energy corresponding to the i^{th} intercalation. Panel (b) shows the probability of successful intercalation as determined by the associated change in free energy using equations 3 and 6.

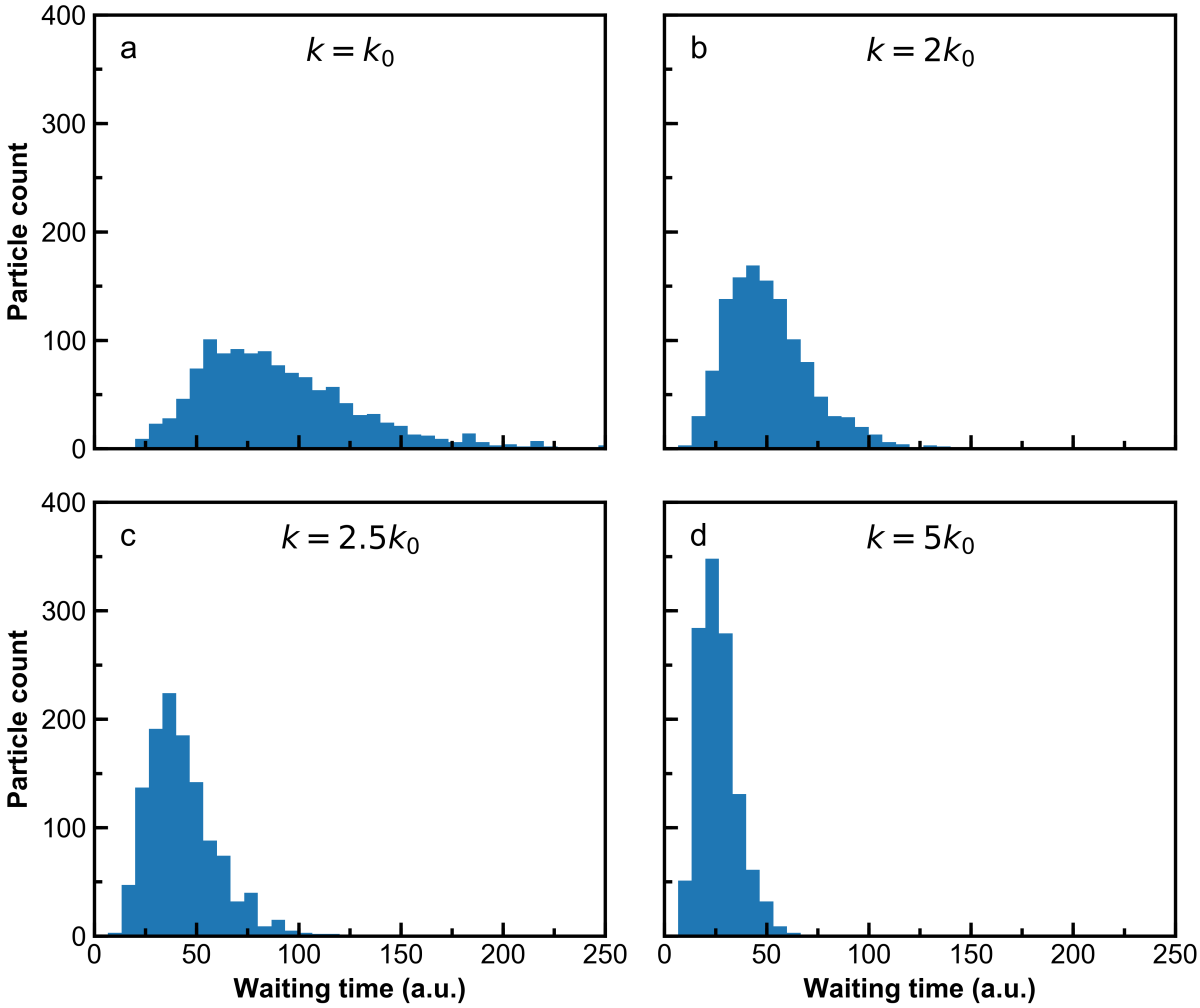

Figure S10. Histograms of waiting times for various initial equilibrium constants that correspond to varied ion concentrations. Each histogram includes 1200 simulated trajectories. The equilibrium constant increases from panels (a) to (d) by the same factors as the CH_3NH_3Br concentration in the experimental data in **Figure 4**. The simulation model used for these plots is the phase-transformation model.

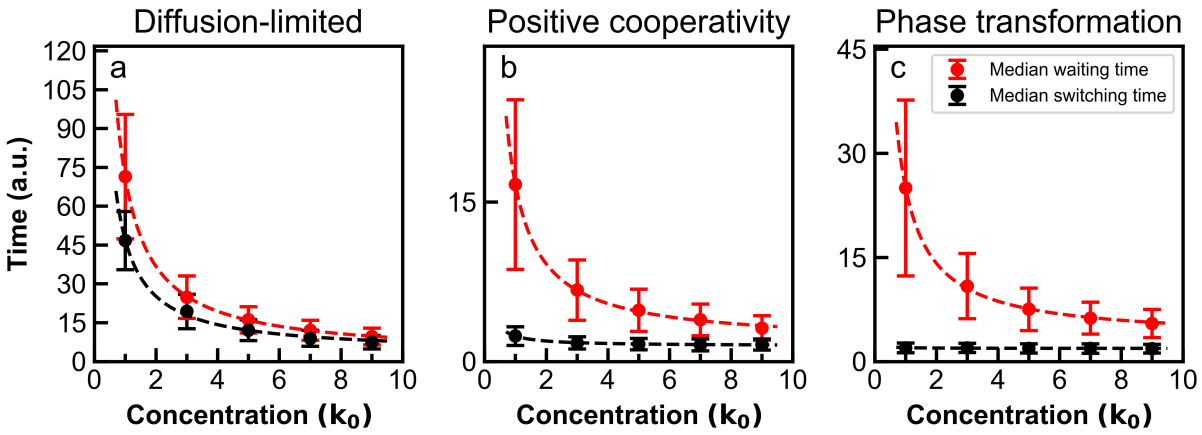

Figure S11. Median waiting and switching times for three different ion-intercalation models. Simulated data are shown for the diffusion-limited, positive-cooperativity, and phase-transformation models in panels (a), (b), and (c), respectively. The error bars correspond to the standard deviation of waiting/switching times for a collection of nanocrystal trajectories. Concentration values are with respect to those used in **Figure 6**. The dashed lines are fits to an inverse proportionality with a constant contribution.

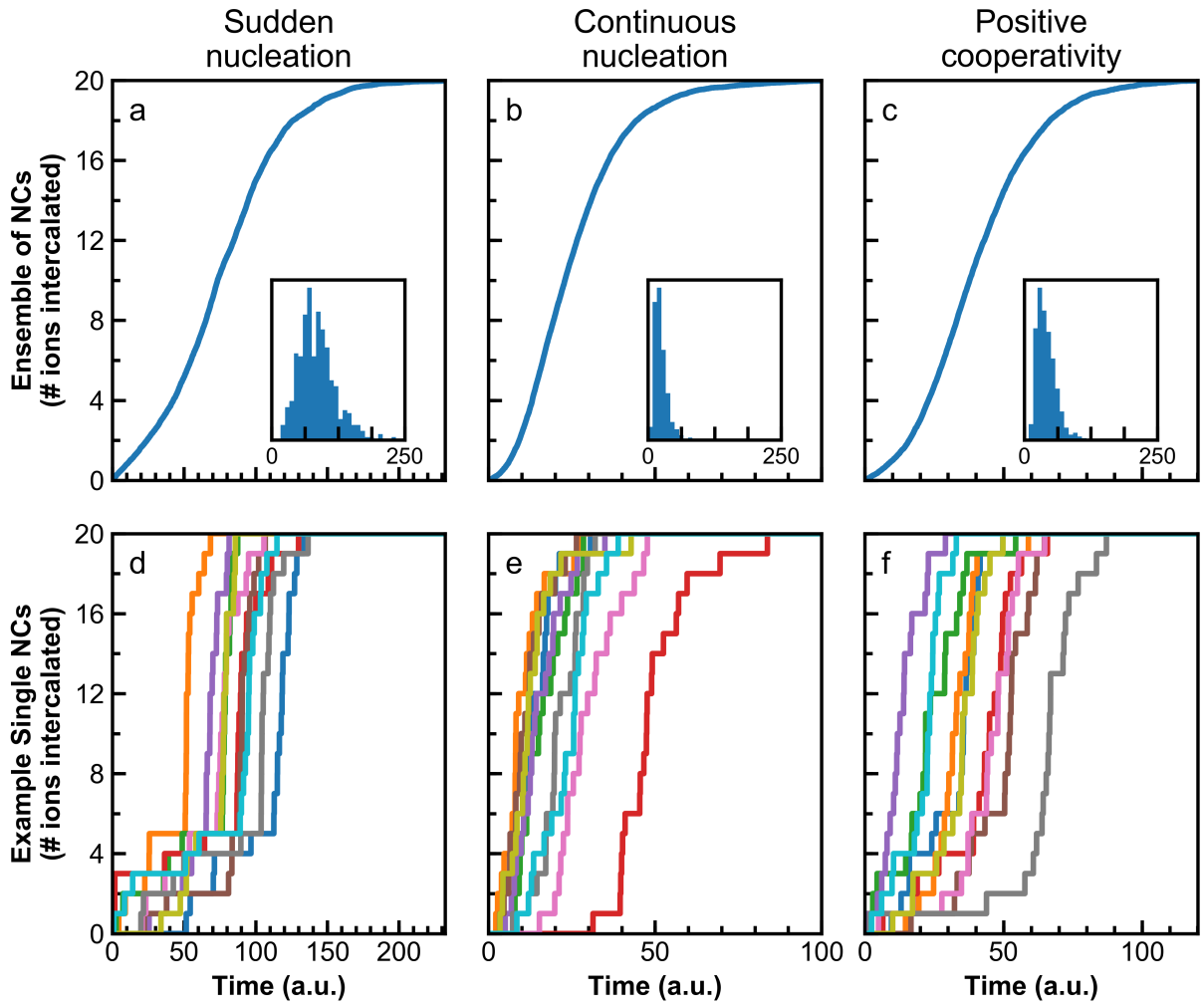

Figure S12. Ensemble and individual intercalation trajectories for three additional models. (a), (b), and (c) show ensemble trajectories for the labeled models with waiting-time histograms inset. (d), (e), and (f) show example individual trajectories for the same three models.

Supplementary References

1. Y. Hassan, Y. Song, R. D. Pensack, A. I. Abdelrahman, Y. Kobayashi, M. A. Winnik and G. D. Scholes, *Advanced Materials*, 2016, **28**, 566-573.
2. M. M. Lee, J. Teuscher, T. Miyasaka, T. N. Murakami and H. J. Snaith, *Science*, 2012, **338**, 643-647.
3. A. V. Naumkin, A. Kraut-Vass, C. J. Powell, S. W. Gaarenstroom, National Institute of Standards and Technology, NIST X-Ray Photoelectron Spectroscopy Database 2012.
4. A. L. Routzahn and P. K. Jain, *Nano Letters*, 2014, **14**, 987-992.
5. W. M. Haynes and D. R. Lide, *CRC Handbook of Chemistry and Physics*, CRC Press, Boca Raton, FL, 2011.
6. D. Pan, Y. Fu, J. Chen, K. J. Czech, J. C. Wright and S. Jin, *Nano Letters*, 2018, **18**, 1807-1813.